

The discovery and characterization of minimoon 2024 PT₅

BRYCE T. BOLIN,^{1,*} LARRY DENNEAU,^{2,*} LAURA-MAY ABRON,³ ROBERT JEDICKE,²
KRISTIN CHIBOUCAS,⁴ CARL INGEBRETSEN,⁵ AND BRIAN C. LEMAUX^{4,6}

¹*Eureka Scientific, Oakland, CA 94602, U.S.A.*

²*Institute for Astronomy, University of Hawai'i at Mānoa, Honolulu, HI, 96822*

³*Griffith Observatory, Los Angeles, CA 90027*

⁴*Gemini Observatory/NSF NOIRLab, Hilo, HI, 96720, USA*

⁵*William H. Miller III Department of Physics and Astronomy, Johns Hopkins University, Baltimore, MD 21218, USA*

⁶*Department of Physics and Astronomy, University of California, Davis, One Shields Ave., Davis, CA 95616, USA*

(Received –; Revised –; Accepted –)

Submitted to ApJL

ABSTRACT

Minimoons are asteroids that become temporarily captured by the Earth-Moon system. We present the discovery of 2024 PT₅, a minimoon discovered by the Asteroid Terrestrial-impact Last Alert System (ATLAS) Sutherland telescope on 2024 August 7. The minimoon with heliocentric semi-major axis, $a \sim 1.01$ au, and perihelion, $q \sim 0.99$ au, became captured by the Earth-Moon system on 2024 September 29 and left on 2024 November 25 UTC. Visible g, r, i, and Z spectrophotometry was obtained using Gemini North/Gemini Multi-Object Spectrograph (GMOS) on 2024 September 27. The color indices are $g-r = 0.58 \pm 0.04$, $r-i = 0.29 \pm 0.04$, $i-Z = -0.27 \pm 0.06$, and the spectrum best matches lunar rock samples followed by S-complex asteroids. Assuming an albedo of 0.21 and using our measured absolute magnitude of 28.64 ± 0.04 , 2024 PT₅ has a diameter of 5.4 ± 1.3 m. We also detect variations in the lightcurve of 2024 PT₅ with a 0.28 ± 0.07 magnitude amplitude and a double-peaked period of $\sim 2600 \pm 500$ s. We improve the orbital solution of 2024 PT₅ with our astrometry and estimate the effect of radiation pressure on its deriving an area-to-mass ratio of $7.02 \pm 2.05 \times 10^{-5}$ m²/kg, implying a density of $\sim 3.9 \pm 2.1$ g/cm³, compatible with having a rocky composition. If we assume 2024 PT₅ is from the NEO population, its most likely sources are resonances in the inner Main Belt by comparing its orbit with the NEO population model, though this does not exclude a lunar origin.

Keywords: minor planets, asteroids: individual (2024 PT₅), temporarily captured orbiters, minimoons

1. INTRODUCTION

* These authors contributed equally to this manuscript.

Evidence from observations of near-Earth objects (NEOs) suggests that the majority originate from the Main Belt asteroids (MBAs) and Jupiter Family Comet (JFC) populations (Granvik et al. 2018; Nesvorný et al. 2023, 2024). A small percentage of NEOs can become temporary Earth co-orbitals, located in a 1:1 mean motion resonance with the Earth (Morais & Morbidelli 2002) where they can become Trojans or quasi-satellites of the Earth for several thousand years (Brasser et al. 2004). A small portion of NEOs, less than 1/10,000,000 of the total NEO population, can become temporarily captured by the Earth-Moon system’s gravity and enter its Hill sphere, becoming a so-called “minimoon” (Granvik et al. 2013; Jedicke et al. 2018).

Minimoons are captured at low relative velocities with the Earth-Moon system, less than 1 km/s, where they can be captured on timescales as long as 10s of days to years (Granvik et al. 2012; Fedorets et al. 2017). The first known minimoon, 2006 RH₁₂₀, remained in orbit around the Earth for \sim 400 days (Kwiatkowski et al. 2008), and the second, 2003 CD₃ was captured for \sim 900 days (Naidu et al. 2021) before escaping the Earth’s Hill sphere. Thus, the capture duration of minimoons represents a small portion of the time they share the Earth’s orbit.

While it is assumed that Earth co-orbitals such as minimoons are captured from the NEO population, emerging evidence suggests that some may originate as lunar impact ejecta. Ejecta from lunar impacts can be re-captured onto Earth-similar orbits where they can last for thousands of years (Gladman et al. 1995). Additionally, the observed spectral properties of some minimoons and quasi-satellites such as 2020 CD₃ and (469219) Kamo’oalewa resemble some lunar samples (Bolin et al. 2020; Sharkey et al. 2021). This evidence has led some to suggest a recent lunar impact as the origin for some Earth co-orbitals (e.g., Jiao et al. 2024)

This paper discusses the discovery of minimoon, 2024 PT₅, by the Asteroid Terrestrial-impact Last Alert System (ATLAS) telescope and observations taken at Gemini North. We will use the approach of Bolin et al. (2021, 2022, 2023) to use spectrophotometric observations at different visible wavelengths to constrain its physical properties as a test of whether 2024 PT₅ has an asteroidal or Lunar debris origin. We will also use the astrometry reported from our observations and the observations of others to refine the orbit of 2024 PT₅, measuring the effect of non-gravitational perturbations on its orbit (e.g., Micheli et al. 2012) and compare its orbit with the NEO population model (Morbidelli et al. 2020; Nesvorný et al. 2023).

2. OBSERVATIONS

The discovery observations of 2024 PT₅ were taken on 2024 August 7 21:11:57 UTC at the ATLAS Sutherland telescope (Minor Planet Center (MPC) observing code M22, Fig. 1, Williams 2024). At the time of the asteroid’s discovery, the asteroid was located at right ascension (RA) = 18 57 04.97, declination = -55 56 00.24 and 1.54 lunar distances (0.00397 au) au from the Earth, a heliocentric distance of 1.017 au, at a phase angle of 128.747°, and had a visible magnitude of \sim 17. The asteroid was detected in four 30 s ATLAS o-band filter exposures spaced over \sim 1700 s. The ATLAS o-band filter provides coverage between 560 nm and 820 nm with an effective wavelength of 663 nm (Tonry et al. 2018). The asteroid was moving 13.7°/d (0.57"/s) in the northwest direction at the time of discovery, resulting in having a trailed appearance in the ATLAS images (panels a, b, c, and d of Fig 1). The trailed exposures of 2024 PT₅ show little to no curvature over the 1700 s span of the discovery detections with a great circle residual of \sim 1.2".

On 2024 September 27 05:54 UTC, 2024 PT₅ was observed using the 8.1 m Gemini North telescope with the Gemini Multi-Object Spectrograph (GMOS) instrument (Hook et al. 2004) in imaging mode

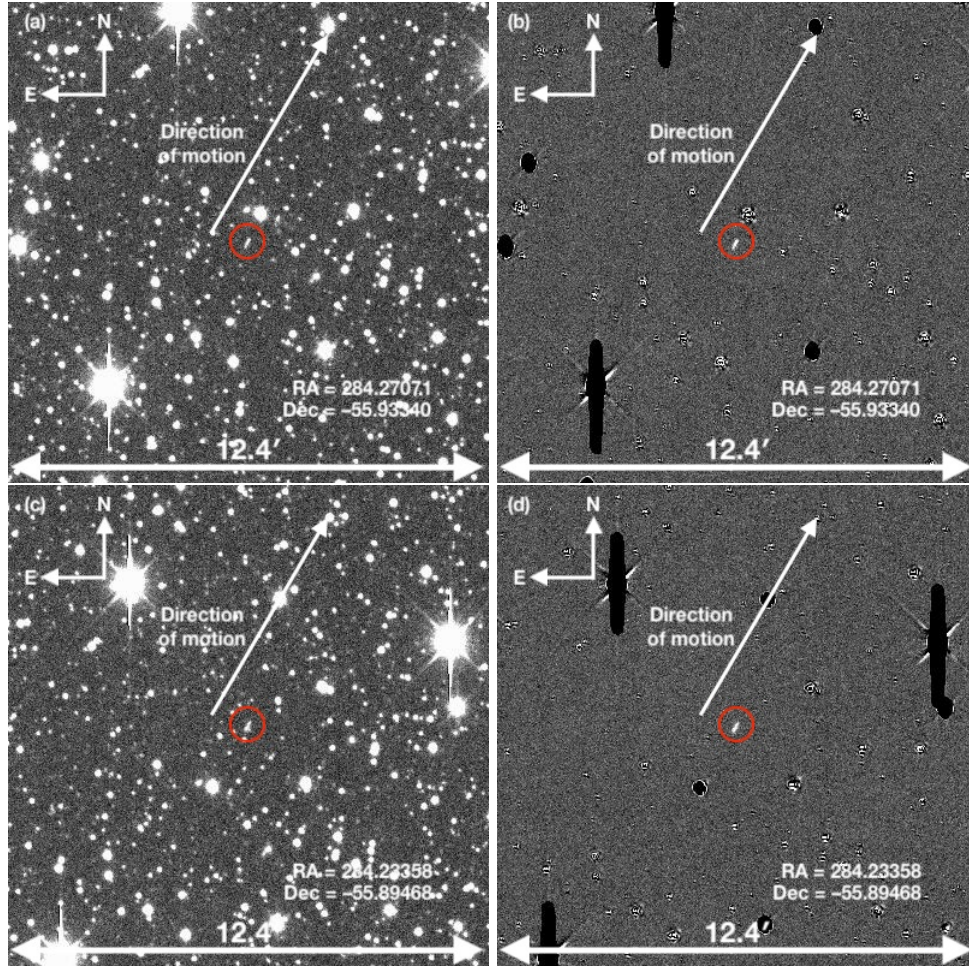


Figure 1. Panel a: The first of four o-band ATLAS-Sutherland telescope discovery images of 2024 PT₅ from 2024 August 7 21:11:57 UTC. The asteroid moved at a rate of 34.3 arcminutes per hour (13.7 degrees per day) in the northwest direction. The asteroid makes a ~ 9 pixel trail in the 30 s ATLAS exposures, indicated by the red circle. **Panel b:** the same as panel a but shows the image after subtracting static sources. Despite the presence of nearby stars, the asteroid is detected cleanly in the subtracted images. **Panel c:** the same as panel a, but the second of four o-band images containing 2024 PT₅ taken on 2024 August 7 21:16:35 UTC. **Panel d:** the same as panel c but shows the image after subtracting static sources. The asteroid was detected with an apparent magnitude of $m=17.13$ in panel b and $m=16.99$ in panel c. The large black areas in the subtracted images are regions of saturated pixels from bright stars. The direction of the asteroid and cardinal directions are indicated in each figure.

(Program ID GN-2024B-FT-106, PI B. Bolin). GMOS was used with the Hamamatsu array with an effective pixel scale of $0.0807''/\text{pixel}$ in 2×2 binning mode. The images were taken in Sloan Digital Sky Survey (SDSS)-equivalent g , r , and i filters (effective wavelengths 0.475 microns, 0.630 microns and 0.780 microns, Fukugita et al. 1996). For coverage of the spectrum of 2024 PT₅ past 0.8 microns, we use the GMOS-N Z-band filter, which is effectively equivalent to the United Kingdom Infrared Telescope Wide-Field Camera (WFCAM) Z filter (Hewett et al. 2006). The WFCAM Z filter (effective wavelength 0.880 microns, Casali et al. 2007) was designed to be equivalent to the SDSS z filter (effective wavelength 0.89 microns) but avoids the atmospheric absorption band near 0.95 microns (Hodgkin et al. 2009).

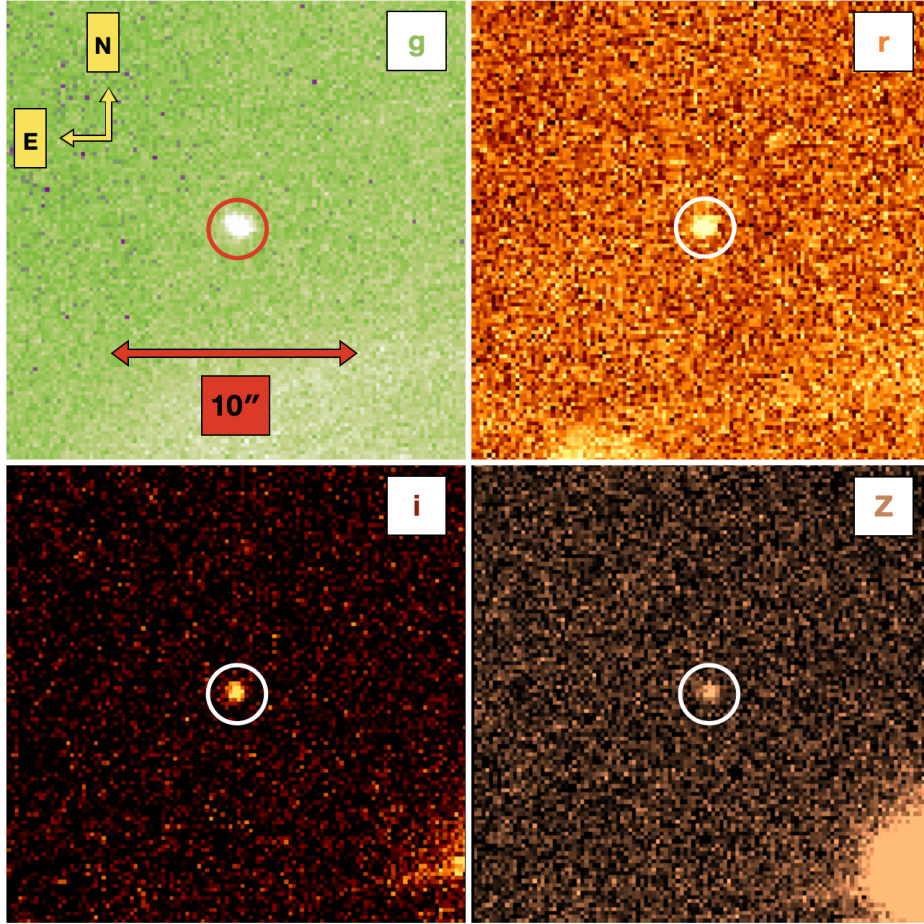


Figure 2. **Top left panel:** a median combination stack of 11 x 75 s g filter images of 2024 PT₅. An arrow indicating the width of 10'' is shown for scale, and the cardinal directions are indicated. **Top right panel:** a median combination stack of 5 x 50 s r filter images of 2024 PT₅. **Bottom left panel:** a median combination stack of 2 x 60 s i filter images of 2024 PT₅. **Bottom right panel:** a median combination stack of 2 x 60 s Z filter images of 2024 PT₅. The image scale and cardinal in the r, i, and Z stacks are the same as in the g image stack.

The observations of 2024 PT₅ with GMOS occurred when it was near RA = 16 59 59.22, dec = +67 01 25.5, 8.74 lunar distances from the Earth (0.0225 au), a heliocentric distance of 1.000 au, and had a phase angle of 84.4°. The seeing was $\sim 0.5\text{-}0.6''$ during the 2024 PT₅ observations as measured in g band images, and airmass ranged from 1.73 -1.91 during the ~ 40 minute observing sequence. During the sequence, we acquired 12 x 75 s g band exposures, 5 x 50 s r band exposures, 3 x 60 s i band exposures, and 3 x 90 s Z band exposures. Observations in the g, r, i, and Z filters were interspersed throughout the observation sequence to mitigate the effects of brightness variations in 2024 PT₅'s lightcurve on the color measurements. The telescope was tracked at the $\sim 93''/\text{h}$ rate of 2024 PT₅ during the exposures. Bias and flat frames were taken and used to detrend the images using the DRAGONS image pipeline (Labrie et al. 2023). Images of 2024 PT₅ when it intersected a background star were discarded. A mosaic of the separate g, r, i, and Z median-combined composite stacks of the 2024 PT₅ images are shown in Fig 2.

3. RESULTS

3.1. Astrometry and orbital determination

The astrometry from the Gemini North observations of 2024 PT₅ was measured with the Astrometrica software (Raab 2012) combined with reference stars from the *Gaia* data release 2 catalog (Gaia Collaboration et al. 2016, 2018). We conservatively estimate an astrometric uncertainty of 1.0'' in both the right ascension and declination directions in line with the typical astrometric precision for most ground-based measurements (e.g., Farnocchia et al. 2022). Additionally, the timing of the GMOS instrument is accurate to within a few tenths of a millisecond, inducing negligible effect on the astrometry¹.

The astrometry measured from the GMOS images was submitted to the MPC (Denneau et al. 2024). The GMOS astrometry of 2024 PT₅ was combined with 200 additional 2024 PT₅ observations taken independently by follow-up observers between 2024 August 7 UTC and 2024 October 24 UTC from the MPC archive². A complete table of the astrometry of 2024 PT₅ is provided in Table A1 of the appendix. We adopt conservative estimates for the astrometric uncertainties of $\sim 1.0''$ in both right ascension and declination for the other observatories' measured positions except for observations made at the Great Shefford Observatory in West Berkshire, England (MPC observatory code J95), where we used an estimated uncertainty of 0.4'' (Vereš et al. 2017).

Using the `Find_Orb` orbital determination software by Bill Gray³, we fit an orbit to the observations in Table A1, using the 8 planets and the Moon as perturbers, and including the effects of solar radiation pressure (e.g., Mommert et al. 2014; Fedorets et al. 2020). Our orbital fit results in estimates of the heliocentric and geocentric semi-major axis, a , eccentricity, e , inclination, i , ascending node, Ω , argument of perihelion, ω , mean anomaly, M , and the area-to-mass ratio (AMR) as a measure of the effect of solar radiation pressure on the orbit of 2024 PT₅.

The heliocentric, geocentric orbital parameters and area-to-mass ratio (a , e , i , Ω , ω , M , AMR) parameter estimates of the least square orbital fit using the observations of 2024 PT₅ is shown in Table 2. The mean observed-minus-computed residual from the least square fit using the 7-parameter fit is 0.33''. A complete list of the observed-minus-computed residuals in the along-track, $X_{res.}$, and cross-track, $Y_{res.}$, are shown in Table A1. The geocentric eccentricity e_g of 2024 PT₅ was ~ 1.05 on 2024 September 27 UTC, the date of the Gemini N observations, indicating that 2024 PT₅ was on a hyperbolic trajectory with respect to Earth. Its AMR of $7.02 \pm 2.05 \times 10^{-5}$ m²/kg is comparable to other small asteroids with measured AMRs (e.g., Micheli et al. 2013; Jedicke et al. 2018).

The orbital trajectory of 2024 PT₅ between 2024 June and 2025 April is shown in Fig. 3 based on values from JPL Horizons⁴. The e_g of 2024 PT₅ decreased below 1.0 at around 2024 September 29 23:40 UTC, as indicated by the red portion of the trajectory of 2024 PT₅ in the top and bottom panels of Fig. 3. The capture of 2024 PT₅ by the Earth-Moon system ended at around 2024 November 25 18:20, making it the most short-lived minimoon known, having been captured by the Earth-moon system for only ~ 60 days. Additionally, 2024 PT₅ did not make a complete revolution around the Earth-Moon barycenter, unlike previous minimoons such as 2006 RH₁₂₀ (Kwiatkowski et al. 2008; Granvik et al. 2012) and 2020 CD₃.

3.2. Photometry and spectral classification

¹ <https://www.gemini.edu/observing/phase-iii-retrieving-reducing-data/reducing-data/timing-information>

² https://minorplanetcenter.net/db_search/show_object?utf8=%E2%9C%93&object_id=2024+PT5, accessed on 2024 November 7.

³ https://www.projectpluto.com/find_orb.htm

⁴ <https://ssd.jpl.nasa.gov/horizons/app.html#/>

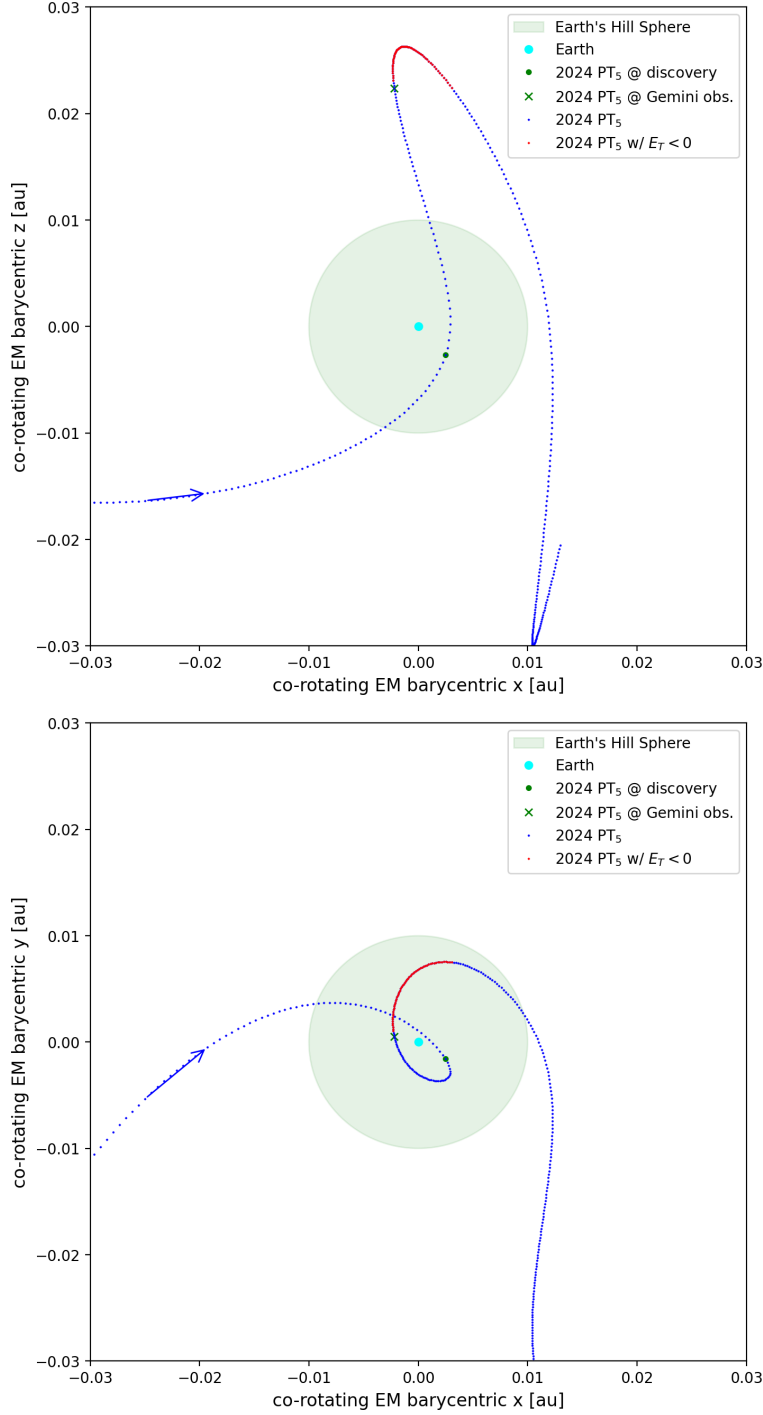


Figure 3. Top panel: side view of the Earth co-rotating frame orbital trajectory of 2024 PT₅ as it enters and leaves the Earth-Moon system between 2024 June and 2025 April in Cartesian Earth-Moon barycentric x and z coordinates. The daily position of 2024 PT₅ is represented as blue points except the portion of its trajectory when it had $e_g < 1$ plotted in red. The position of the Earth is plotted with a cyan circle. The circular green-shaded region indicates the Hill sphere of Earth. The position of 2024 PT₅, when it was discovered, is marked by a green circle, and the position of 2024 PT₅ when Gemini observed it is marked with a green X. A blue arrow indicates the direction of motion of 2024 PT₅ along its orbital path. **Bottom panel:** the same as the top panel, except in Cartesian Earth-Moon barycentric x and y coordinates.

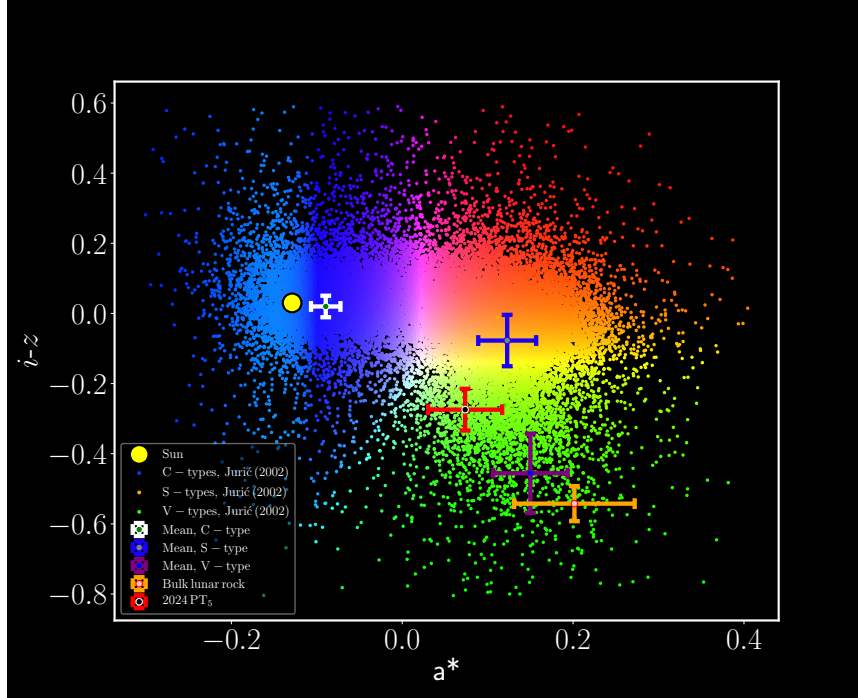


Figure 4. a^* vs. $i-z(Z)$ colors of 2024 PT₅ plotted with a^* vs. $i-z$ colors of C, S and V type asteroids from (Ivezić et al. 2001; Jurić et al. 2002), active comets (Solontoi et al. 2012), and Kuiper Belt Objects (Ofek 2012). The colorization scheme of data points as a function of a^* and $i-z$ is adapted from Ivezić et al. (2002) where blue symbol colors correspond to C-type asteroids, red symbol colors correspond to S-type asteroids and green symbol colors correspond to V-type asteroids. We note that in this case the measured Z magnitude of 2024 PT₅ is plotted as a substitute for its z magnitude. $i-z$. The a^* and $i-z$ range of average S, V, and C-type asteroids are shown computed from the average spectra from DeMeo et al. (2009).

The photometry of 2024 PT₅ was measured using a 0.81'' aperture and then subtracting from it the median contribution from the sky background within a 1.3-2.4'' annulus. The g, r, i, and Z photometry were calibrated using solar analog stars from the Pan-STARRS catalog Chambers et al. (2016). The Pan-STARRS catalog magnitudes of the solar analog stars were transformed to SDSS magnitudes using the conversions from Tonry et al. (2012). We obtained brightnesses of $g = 23.52 \pm 0.03$, $r = 22.95 \pm 0.03$, $i = 22.66 \pm 0.03$, $Z = 22.93 \pm 0.05$. The multi-band colors of 2024 PT₅ are $g-r = 0.58 \pm 0.05$, $r-i = 0.29 \pm 0.04$, and $i-z = -0.27 \pm 0.06$. The g-i color and spectra slope are 0.87 ± 0.04 and $9.5 \pm 1.1\%/100$ nm.

Using the definition of a^* from Ivezić et al. (2001), $a^* = (0.89 (g-r)) + (0.45 (r-i)) - 0.57$, as an indicator of spectral slope, we find $a^* = 0.07 \pm 0.04$ as plotted vs. $i-z(Z)$ in Fig. 4. Overall, 2024 PT₅ has a^* and $i-z$ similar to S-types which have $a^* = 0.12 \pm 0.03$ and $i-z = -0.08 \pm 0.07$ on average and some V-type asteroids which have $a^* = 0.15 \pm 0.11$ and $i-z = -0.46 \pm 0.04$ on average as plotted in Fig. 4. 2024 PT₅ is redder compared with a smaller $i-z$ color compared to C-type asteroids, which have on average an $a^* = -0.09 \pm 0.02$ and $i-z = 0.02 \pm 0.03$ and the Sun, which has an $a^* = -0.13$ and $i-z = 0.03$.

We compute the spectral reflectance of 2024 PT₅ by dividing its flux per g, r, i, and Z filter obtained by the flux of a solar analog in a corresponding filter, normalizing it to a wavelength of 550 nm. The normalized reflectivity spectrum of 2024 PT₅ shown in Fig. 5 is similar to the spectra of S- and V-type

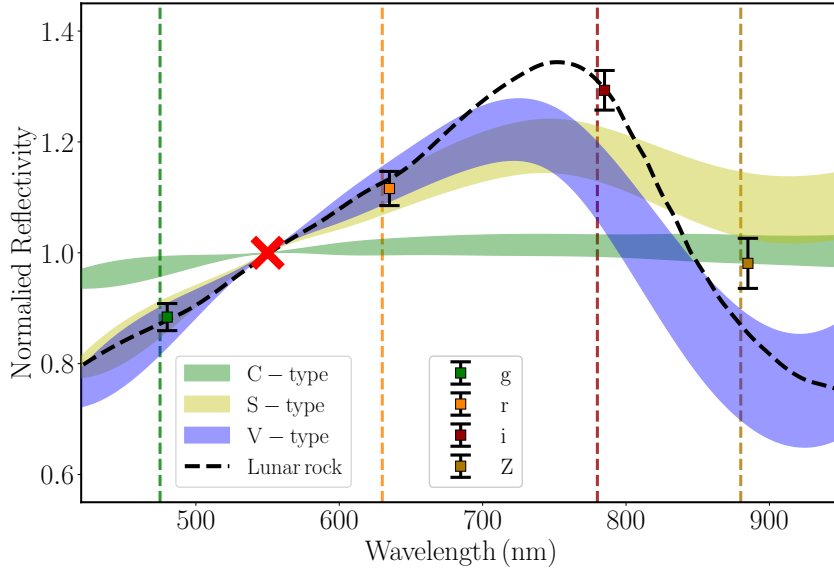


Figure 5. Reflectance photometric spectrum of 2024 PT₅ consisting of g, r, i, and Z observations of 2024 PT₅ on 2024 September 27 UTC. The λ_{eff} locations of the g, r, i, and Z filters have been plotted as vertical dashed lines. The data points for the normalized reflectivity of 2024 PT₅ have been offset slightly from their location in the wavelength direction. The error bars on the spectrum data points correspond to 1σ uncertainty. The spectrum has been normalized to unity at 550 nm, as indicated by the red cross. The spectral range of S, V and C-type asteroids from the Bus-DeMeo asteroid taxonomic catalog (DeMeo et al. 2009) are over-plotted with the V-type spectrum most closely resembling the spectra of 2024 PT₅. The average spectrum of coarse bulk lunar rock samples is plotted for reference (Isaacson et al. 2011).

asteroids (Bus & Binzel 2002; DeMeo et al. 2009) with a red slope between 0.47 microns and 0.77 microns and a decrease in reflectance near 0.88 microns. The spectrum of 2024 PT₅ is also similar to some bulk basaltic lunar rock samples consisting of pyroxene minerals (Isaacson et al. 2011). We compute the χ^2 statistic for the spectrum of 2024 PT₅ compared to the spectrum of 19 different asteroid types including S-complex asteroid types (A, S, Sq, Sv, O, Q, R, V), C-complex types (B, C, Cg, Cgh, D), and X-complex types (K, L, X, Xc, Xe, Xk, Xn) from (DeMeo et al. 2009). We find the closest match is to lunar rock with a reduced χ^2 of 2.76 and Sv-type asteroids with a reduced χ^2 of 3.75.

We use our g and r magnitude measurements of 2024 PT₅ to estimate an equivalent V-band brightness of 23.2 ± 0.04 on 2024 September 7. We calculated the H magnitude of 2024 PT₅ using our estimated V magnitude and the phase function from equation from Bowell et al. (1988):

$$H = V - 5 \log_{10}(r_h \Delta) + 2.5 \log_{10} [(1 - G) \Phi_1(\alpha) + G \Phi_2(\alpha)] \quad (1)$$

where r_h is the 1.000 au heliocentric distance, Δ is its geocentric distance of 0.0225 au and α is its phase angle of 84.4° of 2024 PT₅ on 2024 September 27 UTC. G is the phase coefficient which we use the value of 0.2, the average value for S-type asteroids (Vereš et al. 2015). $\Phi_1(\alpha)$ and $\Phi_2(\alpha)$ are the basis functions normalized at $\alpha = 0^\circ$ described in (Bowell et al. 1988). We obtain $H = 28.64 \pm 0.04$ but caution that the uncertainty on H is underestimated due to the lack of information about the phase function.

3.3. Lightcurve, periodicity, and axial ratio

We use the g filter data to search for periodic variations in the time series brightness of 2024 PT₅. The measured time series photometric values in the individual g images are presented in Table 2 and plotted in the top panel of Fig. 6. There are variations as large as ~ 0.2 - 0.25 magnitudes in the brightness of 2024 PT₅, significantly larger than the ~ 0.01 magnitude variations seen in Skyprobe data for 2024 September 27 UTC⁵ and the ~ 0.05 mag uncertainty of the individual g filter data points.

The Lomb-Scargle periodogram (Lomb 1976) was applied to the time series g filter data, as seen in the top panel of Fig. 7. The highest peak in the lightcurve period vs. spectral power curve is located at ~ 1320 s with a formal significance of $p \simeq 3 \times 10^{-4}$. We apply bootstrap estimation (Press et al. 1986) of the uncertainties by removing \sqrt{N} data points from the time series lightcurve and repeating our periodogram estimation of the lightcurve period 10,000 times, resulting in a central value of ~ 1317 s and a 1σ uncertainty estimate of ~ 227 s. We apply phase dispersion minimization analysis to our data (Stellingwerf 1978) as an independent check of the Lomb-Scargle results, obtaining a result of ~ 1150 s as seen in the bottom panel of Fig. 7, comparable with the lightcurve period estimate. These period estimates imply that 2024 PT₅ has a double-peaked rotation period of $\sim 2600 \pm 500$ s.

Using the observed amplitude of the g filter lightcurve of $0.28 \sim 0.07$, we estimate the rough shape of 2024 PT₅ assuming it is a prolate triaxial ellipsoid with dimensions a:b:c, where $b \geq a \simeq c$ in rough agreement with the shapes of other asteroids inferred from lightcurve inversion (e.g., Hanuš et al. 2016; Hanuš et al. 2018). The ratio between b/a is described by $b/a = 10^{0.4A}$ where A is the peak-to-trough lightcurve amplitude (Binzel et al. 1989) and assuming $a \simeq c$, resulting in a $b/a \sim 1.3$. However, the axial ratio may be exaggerated due to the effect of observing at a large phase angle of $\sim 84^\circ$ on 2024 September 27 UTC (Zappala et al. 1990) as has been suggested for lightcurve observations of other small solar system objects (e.g., Bolin et al. 2018).

4. DISCUSSION AND CONCLUSIONS

The spectrum of 2024 PT₅ is similar to asteroids from the S-complex, as well as some samples of lunar rock, which suggests that it may either originate from the inner Main Belt, where the majority of S-type asteroids are found (DeMeo & Carry 2014), or as a piece of debris resulting from an impact on the moon ejected into an Earth-similar orbit (Gladman et al. 1995). We can use the orbital information of 2024 PT₅ as an additional constraint on its likely origin and physical properties through comparison with dynamical models describing the escape of asteroids from the Main Belt into the NEO population (Granvik et al. 2017; Nesvorný et al. 2023).

Assuming an asteroidal origin for 2024 PT₅, comparison of its orbit with the NEOMOD3 population model suggests its most likely source is the ν_6 resonance located near the inner edge of the Main Belt with an 88.4% probability. The next most likely location, with a 11% chance of 2024 PT₅ coming from it, is the 3:1 mean motion resonance located in the Main Belt at 2.5 au. Weighing the NEO albedo model (Morbidelli et al. 2020) according to these source probabilities for 2024 PT₅ results in a predicted albedo, p_v , of ~ 0.21 , comparable to other small asteroids in the inner Main Belt (Delbo et al. 2003; Binzel et al. 2004).

⁵ https://www.cfht.hawaii.edu/cgi-bin/elixir/skyprobe.pl?plot&mcal_20240927.png

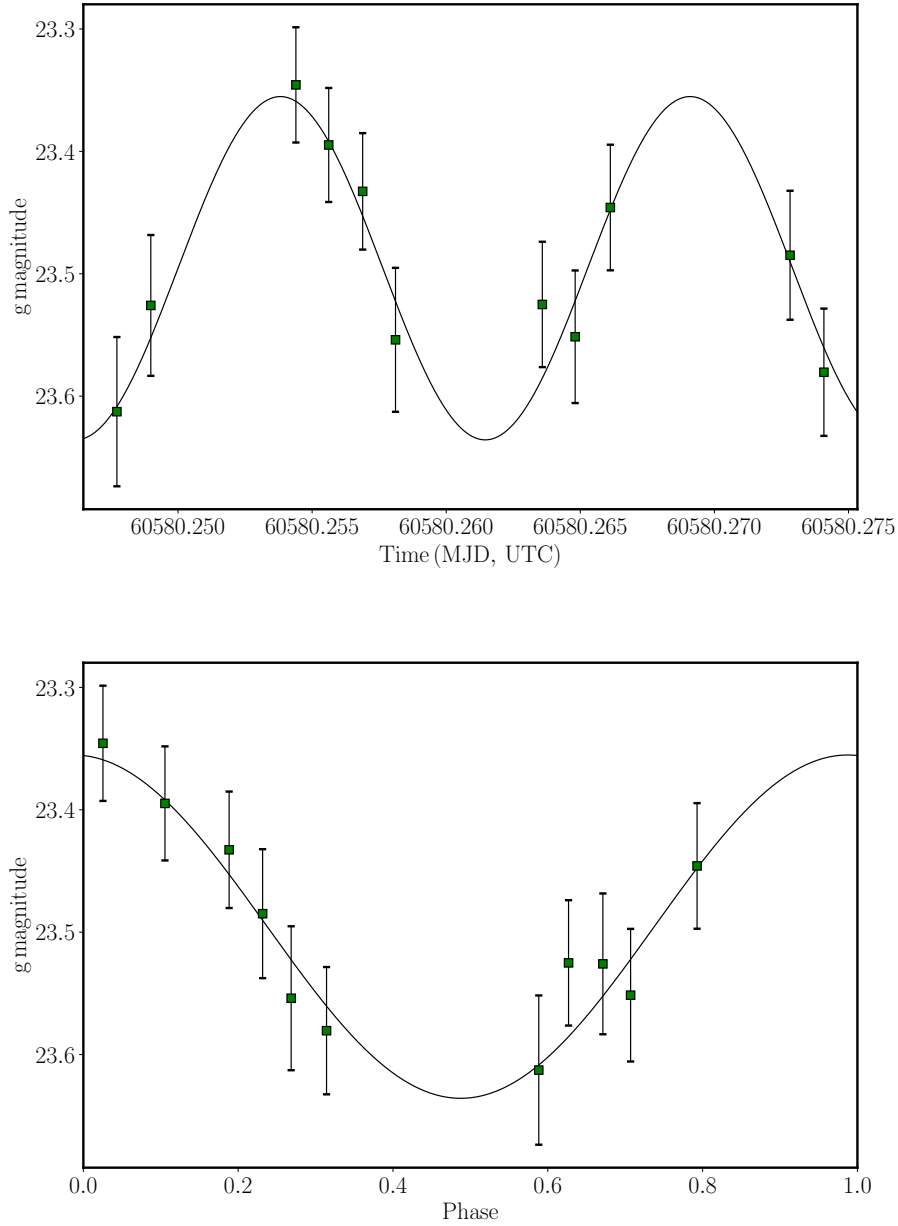


Figure 6. Top panel: g filter lightcurve from 2024 September 27 GMOS observations of 2024 PT₅. The error bars on the data points are equal to their 1σ photometric uncertainties. A model lightcurve is plotted in black with a double-peaked period of ~ 2600 s and amplitude of 0.28 magnitudes. **Bottom panel:** phased g filter lightcurve data of 2024 PT₅ using a lightcurve period of ~ 1300 s and amplitude of 0.28 magnitude.

We use the albedo estimate and H magnitude of 2024 PT₅ to determine the diameter, D , of 2024 PT₅ using the equation $D = \frac{1329}{\sqrt{p_v}} 10^{-\frac{H}{5}}$ from [Russell \(1916\)](#) arriving at $D = 5.4 \pm 1.2$ m. Combining this diameter calculation with the AMR determined from our orbital fit, we can estimate a bulk density for 2024 PT₅ of 3.9 ± 2.1 g/cm³ comparable with achondritic basaltic meteorites ([Macke et al. 2011](#)) and small asteroids with AMR measurements ([Mommert et al. 2014](#)). If we use the mean

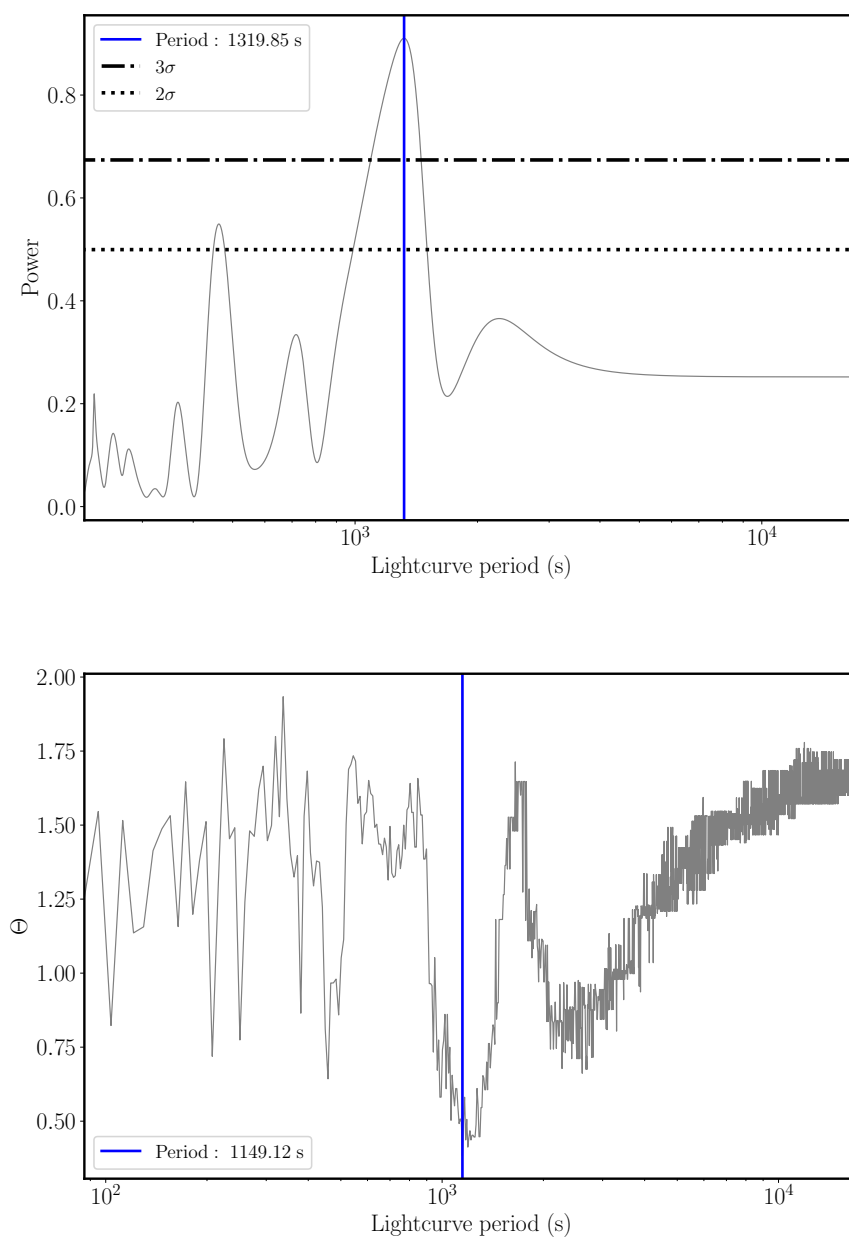


Figure 7. Top panel: Lomb-Scargle periodogram of lightcurve period vs. spectral power (Lomb 1976) for the g filter data from the 2024 September 27 UTC Gemini N/GMOS observations. A peak in the power is located at single-peaked lightcurve period of 1320 s. Bottom panel: Phase dispersion minimization analysis of lightcurve rotation period vs. Θ metric (Stellingwerf 1978). The Θ metric is minimized at single-peaked rotation periods of 1150 s similar to the 1320 ± 227 s period found with the Lomb-Scargle Periodogram.

albedo of lunar surface samples, 0.14 (Matthews 2008), we obtain an diameter of 6.0 ± 1.7 m and a bulk density of $3.6 \pm 2.4 \text{ g/cm}^3$. This density estimate is also comparable to the density of some lunar rock samples (Kiefer et al. 2012). Using this these density estimates, the mass of 2024 PT₅ is $\sim 10^5$ kg. With the comparison of its physical properties determined from our observations to the physical

properties of asteroids and lunar samples, we conclude that 2024 PT₅ the physical properties of 2024 PT₅ deduced from our observations is compatible within an inner Main Belt or lunar ejecta origin.

ACKNOWLEDGMENTS

This study is based on observations obtained at the international Gemini Observatory, a program of NSF's NOIRLab, which is managed by the Association of Universities for Research in Astronomy (AURA) under a cooperative agreement with the National Science Foundation on behalf of the Gemini Observatory partnership.

Gemini Observatory is located on Maunakea, land of the Kānaka Maoli people, and a mountain of considerable cultural, natural, and ecological significance to the indigenous Hawaiian people. The authors wish to acknowledge the importance and reverence of Maunakea and express gratitude for the opportunity to conduct observations from the mountain.

Facility: Gemini North

REFERENCES

- Binzel, R. P., Farinella, P., Zappalà, V., & Cellino, A. 1989, in *Asteroids II*, ed. R. P. Binzel, T. Gehrels, & M. S. Matthews, 416–441
- Binzel, R. P., Rivkin, A. S., Stuart, J. S., et al. 2004, *Icarus*, 170, 259, doi: [10.1016/j.icarus.2004.04.004](https://doi.org/10.1016/j.icarus.2004.04.004)
- Bolin, B. T., Noll, K. S., Caiazzo, I., Fremling, C., & Binzel, R. P. 2023, *Icarus*, 400, 115562, doi: [10.1016/j.icarus.2023.115562](https://doi.org/10.1016/j.icarus.2023.115562)
- Bolin, B. T., Weaver, H. A., Fernandez, Y. R., et al. 2018, *ApJL*, 852, L2, doi: [10.3847/2041-8213/aaa0c9](https://doi.org/10.3847/2041-8213/aaa0c9)
- Bolin, B. T., Fremling, C., Holt, T. R., et al. 2020, *ApJL*, 900, L45, doi: [10.3847/2041-8213/abae69](https://doi.org/10.3847/2041-8213/abae69)
- Bolin, B. T., Fernandez, Y. R., Lisse, C. M., et al. 2021, *AJ*, 161, 116, doi: [10.3847/1538-3881/abd94b](https://doi.org/10.3847/1538-3881/abd94b)
- Bolin, B. T., Ahumada, T., van Dokkum, P., et al. 2022, *MNRAS*, 517, L49, doi: [10.1093/mnrasl/slac089](https://doi.org/10.1093/mnrasl/slac089)
- Bowell, E., Hapke, B., Domingue, D., et al. 1988, *Asteroids II*, 399
- Brasser, R., Innanen, K. A., Connors, M., et al. 2004, *Icarus*, 171, 102, doi: [10.1016/j.icarus.2004.04.019](https://doi.org/10.1016/j.icarus.2004.04.019)
- Bus, S. J., & Binzel, R. P. 2002, *Icarus*, 158, 146, doi: [10.1006/icar.2002.6856](https://doi.org/10.1006/icar.2002.6856)
- Casali, M., Adamson, A., Alves de Oliveira, C., et al. 2007, *A&A*, 467, 777, doi: [10.1051/0004-6361:20066514](https://doi.org/10.1051/0004-6361:20066514)
- Chambers, K. C., Magnier, E. A., Metcalfe, N., et al. 2016, ArXiv e-prints, <https://arxiv.org/abs/1612.05560>
- Delbo, M., Harris, A. W., Binzel, R. P., Pravec, P., & Davies, J. K. 2003, *Icarus*, 166, 116, doi: [10.1016/j.icarus.2003.07.002](https://doi.org/10.1016/j.icarus.2003.07.002)
- DeMeo, F. E., Binzel, R. P., Slivan, S. M., & Bus, S. J. 2009, *Icarus*, 202, 160, doi: [10.1016/j.icarus.2009.02.005](https://doi.org/10.1016/j.icarus.2009.02.005)
- DeMeo, F. E., & Carry, B. 2014, *Nature*, 505, 629, doi: [10.1038/nature12908](https://doi.org/10.1038/nature12908)
- Denneau, L., Siverd, R., Tonry, J., et al. 2024, *Minor Planet Electronic Circulars*, 2024-P170
- Farnocchia, D., Reddy, V., Bauer, J. M., et al. 2022, *Planetary Science Journal*, 3, 156, doi: [10.3847/PSJ/ac7224](https://doi.org/10.3847/PSJ/ac7224)
- Fedorets, G., Granvik, M., & Jedicke, R. 2017, *Icarus*, 285, 83, doi: [10.1016/j.icarus.2016.12.022](https://doi.org/10.1016/j.icarus.2016.12.022)
- Fedorets, G., Micheli, M., Jedicke, R., et al. 2020, *AJ*, 160, 277, doi: [10.3847/1538-3881/abc3bc](https://doi.org/10.3847/1538-3881/abc3bc)
- Fukugita, M., Ichikawa, T., Gunn, J. E., et al. 1996, *AJ*, 111, 1748, doi: [10.1086/117915](https://doi.org/10.1086/117915)
- Gaia Collaboration, Prusti, T., de Bruijne, J. H. J., et al. 2016, *A&A*, 595, A1, doi: [10.1051/0004-6361/201629272](https://doi.org/10.1051/0004-6361/201629272)
- Gaia Collaboration, Brown, A. G. A., Vallenari, A., et al. 2018, *A&A*, 616, A1, doi: [10.1051/0004-6361/201833051](https://doi.org/10.1051/0004-6361/201833051)
- Gladman, B. J., Burns, J. A., Duncan, M. J., & Levison, H. F. 1995, *Icarus*, 118, 302, doi: [10.1006/icar.1995.1193](https://doi.org/10.1006/icar.1995.1193)

- Granvik, M., Jedicke, R., Bolin, B., Chyba, M., & Patterson, G. 2013, *Earth's Temporarily-Captured Natural Satellites - The First Step towards Utilization of Asteroid Resources*, ed. V. Badescu, 151–167
- Granvik, M., Morbidelli, A., Vokrouhlický, D., et al. 2017, *A&A*, 598, A52, doi: [10.1051/0004-6361/201629252](https://doi.org/10.1051/0004-6361/201629252)
- Granvik, M., Vaubaillon, J., & Jedicke, R. 2012, *Icarus*, 218, 262, doi: [10.1016/j.icarus.2011.12.003](https://doi.org/10.1016/j.icarus.2011.12.003)
- Granvik, M., Morbidelli, A., Jedicke, R., et al. 2018, *Icarus*, 312, 181, doi: [10.1016/j.icarus.2018.04.018](https://doi.org/10.1016/j.icarus.2018.04.018)
- Hanuš, J., Delbo, M., Alí-Lagoa, V., et al. 2018, *Icarus*, 299, 84, doi: [10.1016/j.icarus.2017.07.007](https://doi.org/10.1016/j.icarus.2017.07.007)
- Hanuš, J., Delbo, M., Vokrouhlický, D., et al. 2016, *A&A*, 592, A34, doi: [10.1051/0004-6361/201628666](https://doi.org/10.1051/0004-6361/201628666)
- Hewett, P. C., Warren, S. J., Leggett, S. K., & Hodgkin, S. T. 2006, *MNRAS*, 367, 454, doi: [10.1111/j.1365-2966.2005.09969.x](https://doi.org/10.1111/j.1365-2966.2005.09969.x)
- Hodgkin, S. T., Irwin, M. J., Hewett, P. C., & Warren, S. J. 2009, *MNRAS*, 394, 675, doi: [10.1111/j.1365-2966.2008.14387.x](https://doi.org/10.1111/j.1365-2966.2008.14387.x)
- Hook, I. M., Jørgensen, I., Allington-Smith, J. R., et al. 2004, *PASP*, 116, 425, doi: [10.1086/383624](https://doi.org/10.1086/383624)
- Isaacson, P. J., Pieters, C. M., Besse, S., et al. 2011, *Journal of Geophysical Research (Planets)*, 116, E00G11, doi: [10.1029/2010JE003731](https://doi.org/10.1029/2010JE003731)
- Ivezić, Ž., Tabachnik, S., Rafikov, R., et al. 2001, *AJ*, 122, 2749, doi: [10.1086/323452](https://doi.org/10.1086/323452)
- Ivezić, Ž., Lupton, R. H., Jurić, M., et al. 2002, *AJ*, 124, 2943, doi: [10.1086/344077](https://doi.org/10.1086/344077)
- Jedicke, R., Bolin, B. T., Bottke, W. F., et al. 2018, *Frontiers in Astronomy and Space Sciences*, 5, 13, doi: [10.3389/fspas.2018.00013](https://doi.org/10.3389/fspas.2018.00013)
- Jiao, Y., Cheng, B., Huang, Y., et al. 2024, *Nature Astronomy*, 8, 819, doi: [10.1038/s41550-024-02258-z](https://doi.org/10.1038/s41550-024-02258-z)
- Jurić, M., Ivezić, Ž., Lupton, R. H., et al. 2002, *AJ*, 124, 1776, doi: [10.1086/341950](https://doi.org/10.1086/341950)
- Kiefer, W. S., Macke, R. J., Britt, D. T., Irving, A. J., & Consolmagno, G. J. 2012, *Geophys. Res. Lett.*, 39, L07201, doi: [10.1029/2012GL051319](https://doi.org/10.1029/2012GL051319)
- Kwiatkowski, T., Kryszczyńska, A., Polinska, M., et al. 2008, *LPI Contributions*, 1405, 8297
- Labrie, K., Simpson, C., Cardenas, R., et al. 2023, *Research Notes of the American Astronomical Society*, 7, 214, doi: [10.3847/2515-5172/ad0044](https://doi.org/10.3847/2515-5172/ad0044)
- Lomb, N. R. 1976, *Ap&SS*, 39, 447, doi: [10.1007/BF00648343](https://doi.org/10.1007/BF00648343)
- Macke, R. J., Britt, D. T., & Consolmagno, G. J. 2011, *M&PS*, 46, 311, doi: [10.1111/j.1945-5100.2010.01155.x](https://doi.org/10.1111/j.1945-5100.2010.01155.x)
- Matthews, G. 2008, *ApOpt*, 47, 4981, doi: [10.1364/AO.47.004981](https://doi.org/10.1364/AO.47.004981)
- Micheli, M., Tholen, D. J., & Elliott, G. T. 2012, *NewA*, 17, 446, doi: [10.1016/j.newast.2011.11.008](https://doi.org/10.1016/j.newast.2011.11.008)
- . 2013, *Icarus*, 226, 251, doi: [10.1016/j.icarus.2013.05.032](https://doi.org/10.1016/j.icarus.2013.05.032)
- Mommert, M., Hora, J. L., Farnocchia, D., et al. 2014, *ApJ*, 786, 148, doi: [10.1088/0004-637X/786/2/148](https://doi.org/10.1088/0004-637X/786/2/148)
- Morais, M. H. M., & Morbidelli, A. 2002, *Icarus*, 160, 1, doi: [10.1006/icar.2002.6937](https://doi.org/10.1006/icar.2002.6937)
- Morbidelli, A., Delbo, M., Granvik, M., et al. 2020, *Icarus*, 340, 113631, doi: [10.1016/j.icarus.2020.113631](https://doi.org/10.1016/j.icarus.2020.113631)
- Naidu, S. P., Micheli, M., Farnocchia, D., et al. 2021, *ApJL*, 913, L6, doi: [10.3847/2041-8213/abf836](https://doi.org/10.3847/2041-8213/abf836)
- Nesvorný, D., Deienno, R., Bottke, W. F., et al. 2023, *AJ*, 166, 55, doi: [10.3847/1538-3881/ace040](https://doi.org/10.3847/1538-3881/ace040)
- Nesvorný, D., Vokrouhlický, D., Shelly, F., et al. 2024, *Icarus*, 417, 116110, doi: [10.1016/j.icarus.2024.116110](https://doi.org/10.1016/j.icarus.2024.116110)
- Ofek, E. O. 2012, *The Astrophysical Journal*, 749, 10
- Press, W. H., Flannery, B. P., & Teukolsky, S. A. 1986, *Numerical recipes. The art of scientific computing*
- Raab, H. 2012, *Astrometrica: Astrometric data reduction of CCD images*. <http://ascl.net/1203.012>
- Russell, H. N. 1916, *ApJ*, 43, 173, doi: [10.1086/142244](https://doi.org/10.1086/142244)
- Sharkey, B. N. L., Reddy, V., Malhotra, R., et al. 2021, *Communications Earth and Environment*, 2, 231, doi: [10.1038/s43247-021-00303-7](https://doi.org/10.1038/s43247-021-00303-7)
- Solontoi, M., Ivezić, Ž., Jurić, M., et al. 2012, *Icarus*, 218, 571, doi: [10.1016/j.icarus.2011.10.008](https://doi.org/10.1016/j.icarus.2011.10.008)
- Stellingwerf, R. F. 1978, *ApJ*, 224, 953, doi: [10.1086/156444](https://doi.org/10.1086/156444)

- Tonry, J. L., Stubbs, C. W., Lykke, K. R., et al. 2012, *ApJ*, 750, 99, doi: [10.1088/0004-637X/750/2/99](https://doi.org/10.1088/0004-637X/750/2/99)
- Tonry, J. L., Denneau, L., Heinze, A. N., et al. 2018, *PASP*, 130, 064505, doi: [10.1088/1538-3873/aabadf](https://doi.org/10.1088/1538-3873/aabadf)
- Vereš, P., Jedicke, R., Fitzsimmons, A., et al. 2015, *Icarus*, 261, 34, doi: [10.1016/j.icarus.2015.08.007](https://doi.org/10.1016/j.icarus.2015.08.007)
- Vereš, P., Farnocchia, D., Chesley, S. R., & Chamberlin, A. B. 2017, *Icarus*, 296, 139, doi: [10.1016/j.icarus.2017.05.021](https://doi.org/10.1016/j.icarus.2017.05.021)
- Williams, G. V. 2024, *Minor Planet Electronic Circulars*, 2024-V67
- Zappala, V., Cellino, A., Barucci, A. M., Fulchignoni, M., & Lupishko, D. F. 1990, *A&A*, 231, 548

Table 1. Orbital elements of 2024 PT₅ based on observations collected between 2024 August 7 UTC and 2020 October 24 UTC. The orbital elements are shown for the Julian date (JD) using the software `Find_Orb` by Bill Gray. The 1σ uncertainties are given in parentheses.

Heliocentric Elements	
Epoch (JD)	2,460,607.5
Time of perihelion, T_p (JD)	2,460,638.2598770 \pm (5.58x10 ⁻⁵)
Semi-major axis, a (au)	1.0121184340 \pm (2.03x10 ⁻⁸)
Eccentricity, e	0.021315140 \pm (3.89x10 ⁻⁸)
Perihelion, q (au)	0.9905449810 \pm (3.01x10 ⁻⁸)
Aphelion, Q (au)	1.0336918860 \pm (5.53x10 ⁻⁸)
Inclination, i (°)	1.5167380 \pm (4.7x10 ⁻⁶)
Ascending node, Ω (°)	304.494733 \pm (9.0x10 ⁻⁵)
Argument of perihelion, ω (°)	117.54969 \pm (1.0x10 ⁻⁴)
Mean Anomaly, M (°)	330.225693 \pm (5.4x10 ⁻⁵)
Geocentric Elements	
Epoch (JD)	2,460,607.5
Time of perihelion, $T_{p,g}$ (JD)	2,460,429.570191 \pm (2.87x10 ⁻⁴)
Semi-major axis, a_g (au)	0.017623959 \pm (1.09x10 ⁻⁷)
Eccentricity, e_g	0.61405662 \pm (2.04x10 ⁻⁶)
Perihelion, q_g (au)	0.006801850 \pm (7.1x10 ⁻⁸)
Aphelion, Q_g (au)	0.028446068 \pm (1.56x10 ⁻⁷)
Inclination, i_g (°)	105.640940 \pm (4.0x10 ⁻⁵)
Ascending node, Ω_g (°)	302.876944 \pm (3.40x10 ⁻⁴)
Argument of perihelion, ω_g (°)	277.668305 \pm (3.9x10 ⁻⁴)
Mean Anomaly, M_g (°)	129.9004 \pm (1.0x10 ⁻³)
Area-to-Mass ratio, AMR (m ² /kg)	7.02x10 ⁻⁵ \pm (2.05x10 ⁻⁵)
Absolute Magnitude, H	28.64 \pm (0.04)

Table 2. Summary of 2024 PT₅ photometry taken on 2024 September 27 UTC.

Date ¹ (MJD UTC)	Filter ²	Exp ³ (s)	m^4
60580.2477197	g	75 s	23.61 ± 0.06
60580.2489847	g	75 s	23.53 ± 0.06
60580.2543947	g	75 s	23.35 ± 0.05
60580.2556186	g	75 s	23.39 ± 0.05
60580.2568848	g	75 s	23.43 ± 0.05
60580.2581092	g	75 s	23.55 ± 0.06
60580.2635833	g	75 s	23.53 ± 0.05
60580.2648080	g	75 s	23.55 ± 0.05
60580.2661196	g	75 s	23.45 ± 0.05
60580.2728218	g	75 s	23.48 ± 0.05
60580.2740833	g	75 s	23.58 ± 0.05

Table 2. Columns: (1) observation date correct for light travel time; (2) Gemini N/GMOS Filter; (3) Exposure time (4) per filter apparent magnitude with 1 σ uncertainties

APPENDIX

Table A1. Summary of astrometry from observations taken by Keck I/LRIS and other observatories between 2024 August 7 UTC and 2024 October 24 UTC.

Date ¹ (UTC)	R.A. ²	Dec. ³	$\sigma_{\text{R.A.}}$ ⁴ ($''$)	$\sigma_{\text{Dec.}}$ ⁵ ($''$)	$X_{\text{res.}}$ ⁶ ($''$)	$Y_{\text{res.}}$ ⁷ ($''$)	Obs. code ⁸
2024 08 07.883302	18 57 04.970	-55 56 00.24	1.0	1.0	+0.32	-0.59	M22
2024 08 07.886527	18 56 56.059	-55 53 40.85	1.0	1.0	+0.20	-0.33	M22
2024 08 07.892126	18 56 40.711	-55 49 37.52	1.0	1.0	+0.26	-0.23	M22
2024 08 07.903165	18 56 10.685	-55 41 31.85	1.0	1.0	-0.74	-0.31	M22
2024 08 12.060358	18 14 04.848	-09 25 00.44	1.0	1.0	+0.09	+0.44	W68
2024 08 12.065029	18 13 59.820	-09 22 24.35	1.0	1.0	+0.23	-0.25	W68
2024 08 12.070721	18 13 53.688	-09 19 13.58	1.0	1.0	-0.28.	-0.73	W68
2024 08 12.105146	18 13 17.028	-08 59 51.40	1.0	1.0	-0.03	+0.27	W68
2024 08 12.319011	18 12 25.265	-07 31 12.58	1.0	1.0	+0.09	-0.31	T08
2024 08 12.321781	18 12 22.212	-07 29 42.04	1.0	1.0	+0.07	-0.44	T08
2024 08 12.329519	18 12 13.702	-07 25 27.95	1.0	1.0	-0.01	+0.16	T08
2024 08 12.341403	18 12 00.773	-07 18 58.54	1.0	1.0	+0.11	-0.25	T08
2024 08 12.890515	18 09 43.90	-02 45 25.0	1.0	1.0	+0.40	+0.16	I93
2024 08 12.892993	18 09 41.83	-02 44 10.7	1.0	1.0	-0.40	+0.14	I93
2024 08 12.896212	18 09 39.07	-02 42 34.8	1.0	1.0	-0.21	-0.49	I93
2024 08 12.906110	18 08 55.59	-02 37 52.5	1.0	1.0	-0.05	+0.55	M45
2024 08 12.908990	18 08 53.62	-02 36 25.8	1.0	1.0	+0.24	+0.68	M45
2024 08 12.911870	18 08 51.68	-02 34 59.5	1.0	1.0	+0.23	+0.46	M45
2024 08 12.912952	18 09 30.362	-02 36 41.80	0.4	0.4	+0.19	+0.17	J95
2024 08 12.914243	18 09 29.386	-02 36 03.24	0.4	0.4	+0.06	+0.13	J95
2024 08 12.916158	18 09 27.936	-02 35 06.00	0.4	0.4	+0.18	+0.12	J95
2024 08 12.916981	18 09 27.326	-02 34 41.34	0.4	0.4	-0.13	+0.17	J95
2024 08 12.920710	18 08 49.26	-02 30 57.2	1.0	1.0	-0.71	+0.58	L04
2024 08 12.921660	18 09 03.22	-02 29 37.2	1.0	1.0	-0.31	+0.00	126
2024 08 12.924530	18 08 46.74	-02 29 02.7	1.0	1.0	-0.01	+0.56	L04
2024 08 12.925395	18 09 19.685	-02 30 30.96	1.0	1.0	+0.03	+0.31	Z80
2024 08 12.926120	18 08 45.73	-02 28 14.9	1.0	1.0	+0.27	+0.71	L04
2024 08 12.928026	18 09 00.72	-02 26 59.4	1.0	1.0	+0.16	+0.12	203
2024 08 12.929760	18 08 43.40	-02 26 26.1	1.0	1.0	-0.53	+0.48	L04
2024 08 12.930038	18 09 16.248	-02 28 13.04	1.0	1.0	+0.27	-0.42	Z80
2024 08 12.933006	18 08 57.61	-02 24 38.1	1.0	1.0	-0.40	+0.23	204
2024 08 12.934692	18 09 12.878	-02 25 53.69	1.0	1.0	-0.18	+0.03	Z80
2024 08 12.935110	18 08 53.09	-02 22 55.3	1.0	1.0	+0.05	+0.46	126

Continued on next page

Table A1 – *Continued from previous page*

Date ¹ (UTC)	R.A. ²	Dec. ³	$\sigma_{\text{R.A.}}$ ⁴ (")	$\sigma_{\text{Dec.}}$ ⁵ (")	$X_{\text{res.}}$ ⁶ (")	$Y_{\text{res.}}$ ⁷ (")	Obs. code ⁸
2024 08 12.935420	18 08 55.23	-02 23 17.9	1.0	1.0	+0.27	-0.05	203
2024 08 12.936270	18 08 55.21	-02 23 00.8	1.0	1.0	+0.40	+0.31	204
2024 08 12.939514	18 08 52.88	-02 21 23.5	1.0	1.0	+0.18	-0.17	204
2024 08 12.942278	18 08 50.30	-02 19 53.6	1.0	1.0	+0.04	+0.15	203
2024 08 12.942750	18 08 50.56	-02 19 47.0	1.0	1.0	+0.30	+0.08	204
2024 08 12.945971	18 08 48.28	-02 18 10.9	1.0	1.0	+0.20	-0.49	204
2024 08 13.016450	18 09 01.788	-01 10 09.24	1.0	1.0	+0.04	-0.04	Y05
2024 08 13.018163	18 09 00.034	-01 09 18.53	1.0	1.0	-0.34	-0.16	Y05
2024 08 13.019828	18 08 58.400	-01 08 29.81	1.0	1.0	+0.30	+0.00	Y05
2024 08 13.101670	18 08 34.805	-00 23 28.32	1.0	1.0	+0.34	+0.78	W68
2024 08 13.104829	18 08 31.841	-00 21 56.30	1.0	1.0	-0.30	-0.48	W68
2024 08 13.110256	18 08 26.880	-00 19 20.93	1.0	1.0	+0.33	+0.52	W68
2024 08 13.120185	18 08 17.878	-00 14 33.76	1.0	1.0	-0.29	+0.94	W68
2024 08 13.179412	18 07 28.721	+00 13 41.99	1.0	1.0	+0.10	-0.09	W68
2024 08 13.179862	18 07 28.368	+00 13 53.76	1.0	1.0	+0.10	-0.35	W68
2024 08 13.180313	18 07 28.058	+00 14 06.32	1.0	1.0	-0.15	-0.16	W68
2024 08 130.49290	18 08 31.937	-00 09 03.10	1.0	1.0	-0.40	-0.55	U52
2024 08 13.211240	18 08 30.293	-00 08 07.84	1.0	1.0	-0.01	+0.19	U52
2024 08 13.213190	18 08 28.594	-00 07 11.46	1.0	1.0	+0.48	-0.91	U52
2024 08 13.239647	18 09 08.398	+00 15 40.75	1.0	1.0	+0.14	+0.28	T08
2024 08 13.240107	18 09 07.910	+00 15 55.01	1.0	1.0	+0.11	-0.28	T08
2024 08 13.241031	18 09 07.020	+00 16 20.71	1.0	1.0	-0.53	-0.25	T08
2024 08 13.393218	18 06 40.975	+01 27 26.89	1.0	1.0	-0.49	-0.44	T08
2024 08 13.393681	18 06 40.608	+01 27 39.46	1.0	1.0	-0.07	+0.28	T08
2024 08 13.394144	18 06 40.210	+01 27 52.92	1.0	1.0	+0.07	-0.32	T08
2024 08 13.394605	18 06 39.818	+01 28 05.02	1.0	1.0	+0.25	+0.02	T08
2024 08 13.395066	18 06 39.427	+01 28 18.05	1.0	1.0	-0.08	-0.58	T08
2024 08 13.395503	18 06 40.692	+01 27 53.75	1.0	1.0	+0.01	+0.40	T05
2024 08 13.395955	18 06 40.289	+01 28 07.18	1.0	1.0	-0.08	-0.31	T05
2024 08 13.396407	18 06 39.979	+01 28 18.91	1.0	1.0	-0.22	-0.96	T05
2024 08 13.396858	18 06 39.598	+01 28 30.68	1.0	1.0	-0.62	-0.54	T05
2024 08 13.397310	18 06 39.228	+01 28 43.54	1.0	1.0	+0.37	+0.25	T05
2024 08 13.495137	18 07 16.651	+02 06 36.61	1.0	1.0	+0.36	+0.04	Q06
2024 08 131.02696	18 07 1+0.0	+02 10 02.57	1.0	1.0	-0.15	+0.18	Q06
2024 08 13.510252	18 07 03.417	+02 13 28.40	1.0	1.0	-0.28	-0.01	Q06
2024 08 13.818888	18 06 10.31	+04 26 07.1	1.0	1.0	+0.03	-0.03	L01
2024 08 13.820447	18 06 09.10	+04 26 47.6	1.0	1.0	-0.17	-0.05	L01
2024 08 13.822003	18 06 07.91	+04 27 28.0	1.0	1.0	-0.10	+0.41	L01

Continued on next page

Table A1 – *Continued from previous page*

Date ¹ (UTC)	R.A. ²	Dec. ³	$\sigma_{\text{R.A.}}$ ⁴ (")	$\sigma_{\text{Dec.}}$ ⁵ (")	$X_{\text{res.}}$ ⁶ (")	$Y_{\text{res.}}$ ⁷ (")	Obs. code ⁸
2024 08 13.83440	18 06 00.492	+04 30 42.59	1.0	1.0	-0.25	+0.33	G19
2024 08 13.842070	18 05 55.073	+04 34 00.77	1.0	1.0	-0.06	+0.93	G19
2024 08 13.846848	18 05 53.06	+04 38 40.8	1.0	1.0	-0.28	-0.03	104
2024 08 13.850708	18 05 50.09	+04 40 20.6	1.0	1.0	-0.13	+0.25	104
2024 08 13.856160	18 05 45.182	+04 40 04.01	1.0	1.0	+0.07	+0.57	G19
2024 08 13.869870	18 05 35.688	+04 45 55.08	1.0	1.0	+0.04	-0.05	G19
2024 08 13.890150	18 05 21.965	+04 54 32.83	1.0	1.0	-0.53	-0.14	G19
2024 08 13.895540	18 05 18.427	+04 56 49.96	1.0	1.0	-0.37	-0.04	G19
2024 08 13.996440	18 04 13.93	+05 41 28.8	1.0	1.0	-0.28	-0.19	K83
2024 08 13.998900	18 04 12.77	+05 42 28.8	1.0	1.0	-0.14	-0.14	K83
2024 08 14.872873	18 02 20.237	+11 24 21.74	0.4	0.4	-0.07	-0.17	J95
2024 08 14.875193	18 02 18.746	+11 25 12.40	0.4	0.4	-0.18	-0.62	J95
2024 08 14.876750	18 01 52.49	+11 26 12.8	1.0	1.0	+0.13	-0.19	G02
2024 08 14.876922	18 02 17.647	+11 25 50.27	0.4	0.4	-0.11	+0.03	J95
2024 08 14.879154	18 02 16.234	+11 26 39.01	0.4	0.4	+0.05	-0.22	J95
2024 08 14.880290	18 01 50.38	+11 27 29.0	1.0	1.0	0.13	+0.35	G02
2024 08 14.937552	18 01 410.43	+11 51 18.89	1.0	1.0	-0.11	+0.48	Y89
2024 08 14.942425	18 01 37.930	+11 53 02.12	1.0	1.0	+0.01	+0.21	Y89
2024 08 14.947234	18 01 34.727	+11 54 43.23	1.0	1.0	+0.01	-0.03	Y89
2024 08 15.751020	18 00 18.230	+16 56 43.87	1.0	1.0	-0.14	-0.29	M49
2024 08 15.755650	18 00 14.654	+16 58 16.18	1.0	1.0	+0.00	-0.48	M49
2024 08 15.840247	17 59 17.45	+16 54 19.4	1.0	1.0	-0.19	-0.44	G34
2024 08 15.843080	17 59 19.699	+16 55 38.57	1.0	1.0	-0.12	-0.03	K87
2024 08 15.847264	17 59 13.29	+16 56 29.4	1.0	1.0	-0.12	-0.29	G34
2024 08 15.849602	17 59 11.94	+16 57 12.6	1.0	1.0	-0.21	-0.41	G34
2024 08 15.851941	17 59 10.54	+16 57 55.8	1.0	1.0	+0.20	-0.48	G34
2024 08 15.852950	17 59 13.726	+16 58 42.13	1.0	1.0	-0.16	-0.44	K87
2024 08 15.854281	17 59 090.4	+16 58 39.4	1.0	1.0	-0.15	-0.86	Z80
2024 08 15.862810	17 59 07.817	+17 01 45.08	1.0	1.0	+0.29	+0.43	G34
2024 08 16.908094	17 56 12.427	+22 05 37.28	1.0	1.0	-0.24	-0.47	Z80
2024 08 16.919223	17 55 53.02	+22 07 56.8	1.0	1.0	+0.04	+0.26	G34
2024 08 16.919319	17 56 06.643	+22 08 29.15	1.0	1.0	+0.09	+0.97	Z80
2024 08 16.924262	17 55 50.71	+22 09 10.9	1.0	1.0	+0.48	+0.43	G34
2024 08 16.934328	17 55 46.26	+22 11 37.5	1.0	1.0	-0.12	-0.02	G34
2024 08 17.847128	17 54 06.09	+26 04 54.0	1.0	1.0	-0.19	-0.26	203
2024 08 17.866413	17 53 55.23	+26 09 12.6	1.0	1.0	+0.27	-0.97	203
2024 08 19.829362	17 49 49.51	+32 53 05.6	1.0	1.0	-0.17	+0.02	G34
2024 08 19.836813	17 49 45.94	+32 54 22.5	1.0	1.0	+0.01	+0.58	G34

Continued on next page

Table A1 – *Continued from previous page*

Date ¹ (UTC)	R.A. ²	Dec. ³	$\sigma_{\text{R.A.}}$ ⁴ (")	$\sigma_{\text{Dec.}}$ ⁵ (")	$X_{\text{res.}}$ ⁶ (")	$Y_{\text{res.}}$ ⁷ (")	Obs. code ⁸
2024 08 19.844249	17 49 42.41	+32 55 37.3	1.0	1.0	+0.13	+0.12	G34
2024 08 19.851685	17 49 38.86	+32 56 50.8	1.0	1.0	-0.53	-0.71	G34
2024 08 23.848972	17 42 22.905	+42 36 29.87	1.0	1.0	+0.10	-0.28	Z84
2024 08 23.855223	17 42 19.625	+42 37 09.02	1.0	1.0	-0.05	-0.15	Z84
2024 08 27.821450	17 35 51.09	+48 46 30.6	1.0	1.0	-0.05	+0.00	033
2024 08 27.822600	17 35 50.65	+48 46 35.0	1.0	1.0	-0.01	-0.04	033
2024 08 27.823740	17 35 500.4	+48 46 39.5	1.0	1.0	-0.12	+0.09	033
2024 08 28.837555	17 34 24.755	+50 04 53.76	1.0	1.0	+0.11	-0.01	Z84
2024 08 28.847621	17 34 20.044	+50 05 29.17	1.0	1.0	-0.09	-0.07	Z84
2024 08 28.858796	17 34 14.908	+50 06 06.48	1.0	1.0	-0.23	-0.02	Z84
2024 09 10.858840	17 20 371.0	+60 13 29.6	1.0	1.0	-0.32	-0.27	Y65
2024 09 10.861540	17 20 36.47	+60 13 32.6	1.0	1.0	+0.06	+0.18	Y66
2024 09 10.881860	17 20 28.45	+60 13 48.9	1.0	1.0	-0.89	+0.63	Y65
2024 09 10.893360	17 20 24.45	+60 13 56.6	1.0	1.0	+0.94	+0.61	Y65
2024 09 10.894970	17 20 23.77	+60 13 57.4	1.0	1.0	+0.20	+0.59	Y64
2024 09 10.902740	17 20 21.01	+60 14 01.3	1.0	1.0	+0.10	-0.26	Y64
2024 09 10.903640	17 20 20.68	+60 14 02.1	1.0	1.0	-0.03	+0.34	Y66
2024 09 10.904870	17 20 20.36	+60 14 02.6	1.0	1.0	+0.76	+0.26	Y65
2024 09 10.917350	17 20 16.11	+60 14 06.8	1.0	1.0	+0.21	+0.64	Y65
2024 09 10.926880	17 20 13.07	+60 14 08.0	1.0	1.0	+0.02	+0.28	Y64
2024 09 10.929830	17 20 12.27	+60 14 07.9	1.0	1.0	+0.06	+0.25	Y65
2024 09 10.935310	17 20 10.52	+60 14 09.6	1.0	1.0	+0.89	+0.33	Y64
2024 09 10.941530	17 20 08.71	+60 14 09.8	1.0	1.0	+0.94	+0.01	Y66
2024 09 10.943320	17 20 08.32	+60 14 10.2	1.0	1.0	+0.52	+0.54	Y64
2024 09 10.950330	17 20 06.39	+60 14 09.6	1.0	1.0	+0.28	+0.42	Y64
2024 09 10.957410	17 20 04.60	+60 14 08.9	1.0	1.0	+0.48	+0.51	Y64
2024 09 10.965050	17 20 02.72	+60 14 07.8	1.0	1.0	+0.22	+0.33	Y64
2024 09 10.972070	17 20 01.09	+60 14 06.0	1.0	1.0	-0.10	+0.20	Y64
2024 09 10.979490	17 19 59.49	+60 14 04.6	1.0	1.0	-0.39	+0.35	Y64
2024 09 11.845450	17 19 52.21	+60 45 30.9	1.0	1.0	-0.03	-0.42	Y65
2024 09 11.856860	17 19 47.59	+60 45 43.7	1.0	1.0	-0.04	+0.24	Y65
2024 09 11.860860	17 19 45.98	+60 45 47.1	1.0	1.0	+0.26	+0.02	Y66
2024 09 11.879880	17 19 38.65	+60 46 01.8	1.0	1.0	-0.19	+0.38	Y65
2024 09 11.891390	17 19 34.52	+60 46 07.8	1.0	1.0	+0.47	-0.35	Y65
2024 09 11.895360	17 19 33.04	+60 46 12.0	1.0	1.0	+0.18	+0.44	Y64
2024 09 11.934030	17 19 20.61	+60 46 17.6	1.0	1.0	+0.23	+0.11	Y65
2024 09 11.940900	17 19 18.68	+60 46 18.7	1.0	1.0	-0.45	+0.38	Y66
2024 09 11.972740	17 19 10.92	+60 46 13.4	1.0	1.0	+0.18	+0.24	Y64

Continued on next page

Table A1 – *Continued from previous page*

Date ¹ (UTC)	R.A. ²	Dec. ³	$\sigma_{\text{R.A.}}$ ⁴ (")	$\sigma_{\text{Dec.}}$ ⁵ (")	$X_{\text{res.}}$ ⁶ (")	$Y_{\text{res.}}$ ⁷ (")	Obs. code ⁸
2024 09 12.843360	17 19 01.18	+61 16 43.2	1.0	1.0	+0.23	+0.08	Y65
2024 09 12.854770	17 18 56.48	+61 16 54.7	1.0	1.0	-0.45	+0.24	Y65
2024 09 12.866280	17 18 52.04	+61 17 03.7	1.0	1.0	+0.11	-0.03	Y65
2024 09 12.877790	17 18 47.64	+61 17 11.8	1.0	1.0	-0.09	+0.44	Y65
2024 09 12.889300	17 18 43.44	+61 17 17.4	1.0	1.0	-0.07	+0.11	Y65
2024 09 12.900810	17 18 39.48	+61 17 21.3	1.0	1.0	+0.33	-0.30	Y65
2024 09 12.912440	17 18 35.66	+61 17 23.7	1.0	1.0	+0.55	-0.70	Y65
2024 09 12.927820	17 18 30.86	+61 17 25.8	1.0	1.0	+0.12	-0.08	Y65
2024 09 13.848500	17 18 05.30	+61 47 03.9	1.0	1.0	+0.38	+0.24	Y65
2024 09 13.867540	17 17 57.79	+61 47 18.3	1.0	1.0	+0.13	+0.58	Y65
2024 09 13.887930	17 17 50.30	+61 47 28.7	1.0	1.0	+0.44	+0.42	Y65
2024 09 15.844340	17 16 10.55	+62 44 45.7	1.0	1.0	-0.01	+0.14	Y65
2024 09 15.863380	17 16 03.04	+62 44 58.2	1.0	1.0	+0.02	+0.04	Y65
2024 09 15.883760	17 15 55.46	+62 45 06.3	1.0	1.0	-0.11	-0.13	Y65
2024 09 17.843650	17 13 58.40	+63 38 52.7	1.0	1.0	-0.85	+0.65	Y65
2024 09 17.860820	17 13 51.66	+63 39 01.1	1.0	1.0	-0.40	-0.58	Y65
2024 09 20.861960	17 09 58.04	+64 52 53.6	1.0	1.0	+0.26	-0.58	Y65
2024 09 20.877340	17 09 52.26	+64 52 55.3	1.0	1.0	-0.12	+0.04	Y65
2024 09 20.890480	17 09 47.64	+64 52 53.7	1.0	1.0	-0.01	+0.06	Y65
2024 09 21.843050	17 08 39.12	+65 15 27.1	1.0	1.0	+0.02	+0.08	Y65
2024 09 21.864780	17 08 30.58	+65 15 30.0	1.0	1.0	-0.11	+0.44	Y65
2024 09 21.889660	17 08 21.65	+65 15 26.4	1.0	1.0	-0.23	-0.65	Y65
2024 09 22.841140	17 07 1+0.	+65 37 03.7	1.0	1.0	-0.40	+0.20	Y65
2024 09 22.865190	17 07 00.66	+65 37 04.4	1.0	1.0	+0.26	-0.10	Y65
2024 09 23.842030	17 05 36.94	+65 57 41.1	1.0	1.0	-0.12	+0.31	Y65
2024 09 23.871830	17 05 25.56	+65 57 39.0	1.0	1.0	-0.28	+0.16	Y65
2024 09 24.838390	17 04 03.45	+66 17 22.4	1.0	1.0	+0.02	+0.12	Y65
2024 09 24.855550	17 03 56.71	+66 17 21.9	1.0	1.0	-0.08	+0.20	Y65
2024 09 24.872030	17 03 50.62	+66 17 18.2	1.0	1.0	-0.23	+0.24	Y65
2024 09 25.83630	17 02 27.43	+66 36 11.3	1.0	1.0	-0.29	+0.52	Y65
2024 09 25.852330	17 02 21.15	+66 36 09.6	1.0	1.0	+0.14	+0.02	Y65
2024 09 25.868470	17 02 15.17	+66 36 05.0	1.0	1.0	-0.08	-0.31	Y65
2024 09 26.834820	17 00 49.93	+66 54 10.9	1.0	1.0	+0.09	-0.16	Y65
2024 09 26.850110	17 00 43.91	+66 54 08.8	1.0	1.0	-0.01	+0.12	Y65
2024 09 26.86550	17 00 38.26	+66 54 04.2	1.0	1.0	+0.45	+0.40	Y65
2024 09 26.886340	17 00 31.16	+66 53 54.6	1.0	1.0	+0.37	+0.44	Y65
2024 09 26.907180	17 00 25.01	+66 53 40.9	1.0	1.0	-0.02	-0.52	Y65
2024 09 26.951330	17 00 14.74	+66 53 06.0	1.0	1.0	+0.16	+0.05	Y65

Continued on next page

Table A1 – *Continued from previous page*

Date ¹ (UTC)	R.A. ²	Dec. ³	$\sigma_{\text{R.A.}}$ ⁴ (")	$\sigma_{\text{Dec.}}$ ⁵ (")	$X_{\text{res.}}$ ⁶ (")	$Y_{\text{res.}}$ ⁷ (")	Obs. code ⁸
2024 09 27.246150	16 59 59.22	+67 01 25.5	1.0	1.0	-0.34	-0.29	T15
2024 09 27.252830	16 59 56.71	+67 01 22.3	1.0	1.0	-0.37	-0.29	T15
2024 09 27.259010	16 59 54.45	+67 01 19.0	1.0	1.0	-0.46	-0.26	T15
2024 09 27.833970	16 59 11.15	+67 11 26.6	1.0	1.0	-0.08	+0.57	Y65
2024 09 27.838560	16 59 09.40	+67 11 25.9	1.0	1.0	+0.32	+0.37	Y66
2024 09 27.845560	16 59 06.71	+67 11 24.4	1.0	1.0	+0.46	+0.18	Y64
2024 09 27.853000	16 59 03.82	+67 11 21.8	1.0	1.0	-0.03	+0.18	Y65
2024 09 27.866620	16 58 58.90	+67 11 16.8	1.0	1.0	-0.13	+0.07	Y66
2024 09 27.868700	16 58 58.19	+67 11 15.9	1.0	1.0	-0.07	+0.25	Y64
2024 09 27.878680	16 58 54.83	+67 11 10.9	1.0	1.0	-0.11	+0.19	Y65
2024 09 27.890840	16 58 50.98	+67 11 03.9	1.0	1.0	-0.20	+0.29	Y64
2024 09 27.896790	16 58 49.24	+67 10 59.8	1.0	1.0	-0.01	+0.33	Y66
2024 09 27.913480	16 58 44.60	+67 10 47.5	1.0	1.0	-0.31	+0.29	Y64
2024 09 28.834420	16 57 31.24	+67 28 00.7	1.0	1.0	+0.12	+0.55	Y65
2024 09 28.883810	16 57 13.72	+67 27 39.0	1.0	1.0	+0.00	-0.07	Y65
2024 09 28.895290	16 57 11.15	+67 27 36.2	1.0	1.0	-0.47	+0.18	950
2024 09 28.901770	16 57 09.31	+67 27 31.6	1.0	1.0	-0.32	+0.19	950
2024 09 28.908250	16 57 07.51	+67 27 26.9	1.0	1.0	-0.42	+0.13	950
2024 09 28.914730	16 57 05.83	+67 27 21.9	1.0	1.0	-0.33	+0.06	950
2024 09 28.921220	16 57 04.32	+67 27 16.6	1.0	1.0	-0.23	+0.57	950
2024 09 28.927700	16 57 02.74	+67 27 11.4	1.0	1.0	-0.13	+0.22	950
2024 09 29.829060	16 55 53.02	+67 44 00.0	1.0	1.0	-0.16	+0.35	Y65
2024 09 29.848470	16 55 45.62	+67 43 53.9	1.0	1.0	-0.04	+0.02	Y65
2024 10 01.837490	16 52 27.89	+68 14 20.4	1.0	1.0	+0.00	+0.08	Y65
2024 10 01.859730	16 52 20.02	+68 14 08.9	1.0	1.0	+0.17	-0.13	Y65
2024 10 01.881990	16 52 12.98	+68 13 54.1	1.0	1.0	-0.02	+0.22	Y65
2024 10 04.839290	16 47 19.41	+68 56 55.2	1.0	1.0	+0.26	-0.42	Y65
2024 10 04.885480	16 47 05.00	+68 56 22.5	1.0	1.0	+0.22	-0.12	Y65
2024 10 04.932390	16 46 54.96	+68 55 37.7	1.0	1.0	+0.13	-0.16	Y65
2024 10 05.849080	16 45 31.01	+69 10 26.6	1.0	1.0	+0.22	-0.61	Y65
2024 10 05.888130	16 45 19.54	+69 09 55.9	1.0	1.0	+0.27	-0.26	Y65
2024 10 05.929280	16 45 11.08	+69 09 15.9	1.0	1.0	+0.66	-0.60	Y65
2024 10 07.882960	16 41 45.06	+69 36 32.0	1.0	1.0	-0.73	-0.11	Y65
2024 10 07.892370	16 41 42.59	+69 36 23.9	1.0	1.0	+0.24	+0.40	Y65
2024 10 08.828320	16 40 09.68	+69 50 13.4	1.0	1.0	+0.65	+0.64	Y65
2024 10 08.845860	16 40 03.75	+69 50 01.4	1.0	1.0	-0.08	-0.14	Y65
2024 10 08.861730	16 39 58.69	+69 49 48.6	1.0	1.0	+0.48	-0.35	Y65
2024 10 09.845230	16 38 08.18	+70 02 50.4	1.0	1.0	+0.64	+0.57	Y65

Continued on next page

Table A1 – *Continued from previous page*

Date ¹ (UTC)	R.A. ²	Dec. ³	$\sigma_{\text{R.A.}}$ ⁴ (")	$\sigma_{\text{Dec.}}$ ⁵ (")	$X_{\text{res.}}$ ⁶ (")	$Y_{\text{res.}}$ ⁷ (")	Obs. code ⁸
2024 10 09.881260	16 37 57.91	+70 02 18.8	1.0	1.0	-0.30	+0.26	Y65
2024 10 09.918150	16 37 50.18	+70 01 42.8	1.0	1.0	-0.26	-0.60	Y65
2024 10 10.880560	16 35 58.18	+70 14 55.4	1.0	1.0	+0.16	+0.11	Y65
2024 10 10.917460	16 35 50.83	+70 14 18.0	1.0	1.0	-0.26	-0.40	Y65
2024 10 14.847810	16 27 15.74	+71 03 22.0	1.0	1.0	+0.16	-0.64	Y65
2024 10 14.893390	16 27 04.32	+71 02 35.6	1.0	1.0	-0.63	-0.14	Y65
2024 10 18.846060	16 16 51.10	+71 44 58.1	1.0	1.0	+0.27	-0.35	Y65
2024 10 18.885080	16 16 41.38	+71 44 12.4	1.0	1.0	+0.40	+0.57	Y65
2024 10 19.843800	16 14 03.17	+71 54 01.4	1.0	1.0	-0.36	-0.26	Y66
2024 10 22.851930	16 05 19.37	+72 17 31.3	1.0	1.0	+0.18	+0.05	Y65
2024 10 22.870340	16 05 15.17	+72 17 09.0	1.0	1.0	-0.05	-0.64	Y65
2024 10 24.843290	15 59 28.11	+72 31 02.0	1.0	1.0	+0.92	-0.43	Y65
2024 10 24.859690	15 59 24.31	+72 30 40.0	1.0	1.0	+0.20	-0.41	Y65

Table A1. Columns: (1) UTC observation date at the mid-point of the exposure; (2) right ascension; (3) declination; (4) uncertainty in right ascension; (5) uncertainty in declination; (6) observed-minus-computed residual in the X direction; (7) observed-minus-computed residual in the Y direction; (8) Minor Planet Center Observatory Code